

Technical Note

Integration of Modified Solvay Process for Sodium Bicarbonate Synthesis from Saline Brines with Steelmaking for Utilization of Electric Arc Furnace Slag in CO₂ Sequestration and Reagent Regeneration

Shadman Monir Anto, Asif Ali and Rafael M. Santos * 

School of Engineering, University of Guelph, Guelph, ON N1G 2W1, Canada; antos@uoguelph.ca (S.M.A.); aali38@uoguelph.ca (A.A.)

* Correspondence: santosr@uoguelph.ca; Tel.: +1-519-824-4120

Abstract: In the pursuit of sustainable solutions for carbon dioxide CO₂ sequestration and emission reduction in the steel industry, this study presents an innovative integration of steelmaking slag with the modified Solvay process for sodium bicarbonate (NaHCO₃) synthesis from saline brines. Utilizing diverse minerals, including electric arc furnace (EAF) slag, olivine, and kimberlite, the study explored their reactivity under varied pH conditions and examined their potential in ammonium regeneration. SEM and WDXRF analyses were utilized to acquire morphological and chemical compositions of the minerals. Advanced techniques such as XRD and ICP-OES were employed to meticulously analyze mineralogical transformations and elemental concentrations. The findings demonstrate that steelmaking slag, owing to its superior reactivity and pH buffering capabilities, outperforms natural minerals. The integration of finer slag particles significantly elevated pH levels, facilitating efficient ammonium regeneration. Geochemical modeling provided valuable insights into mineral stability and reactivity, which aligned with the ICP-OES results. This synergistic approach not only aids in CO₂ capture through mineral carbonation but also minimizes waste, showcasing its potential as a sustainable and environmentally responsible solution for CO₂ mitigation in the steel industry.

Keywords: carbon capture; utilization; and sequestration; mineral carbonation; ammonium regeneration; steelmaking; EAF slag; climate change



Citation: Anto, S.M.; Ali, A.; Santos, R.M. Integration of Modified Solvay Process for Sodium Bicarbonate Synthesis from Saline Brines with Steelmaking for Utilization of Electric Arc Furnace Slag in CO₂ Sequestration and Reagent Regeneration. *Minerals* **2024**, *14*, 97. <https://doi.org/10.3390/min14010097>

Academic Editor: Tuncel M. Yegulalp

Received: 29 October 2023

Revised: 24 December 2023

Accepted: 4 January 2024

Published: 16 January 2024

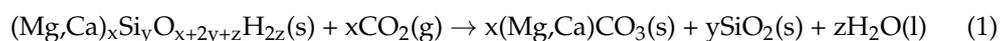


Copyright: © 2024 by the authors. Licensee MDPI, Basel, Switzerland. This article is an open access article distributed under the terms and conditions of the Creative Commons Attribution (CC BY) license (<https://creativecommons.org/licenses/by/4.0/>).

1. Introduction

Climate change is an escalating crisis, causing global warming by rising levels of CO₂ in the atmosphere, having surpassed 424 ppm in 2023, largely due to burning fossil fuels [1–4]. Reducing greenhouse gas emissions has become a top priority for industries, especially the iron and steel sector, which is the world’s largest consumer of energy [5]. In 2020 alone, global steel production reached a staggering 1.878 billion tons, as reported by the World Steel Association (WSA) [6]. Despite steel’s recyclability, its production process remains notorious for its immense energy consumption and carbon intensity [7]. Remarkably, the greenhouse gases emitted from steelmaking activities account for a substantial portion, approximately 2.8 billion tons, constituting 5.5%–6% of the world’s annual greenhouse gas emissions [8,9]. One potential solution to reduce steelmaking emissions is mineral carbonation, a technology that captures CO₂ [10,11]. Numerous scholars have extensively researched CO₂ sequestration through steel slag carbonation, exploring its economic benefits and applications in construction and green materials [12]. However, a critical evaluation of various carbonation methods’ impacts on steel slag, comparative performance analysis of resulting products, and assessment of industrialization challenges are still active areas in ongoing research [10].

The fundamental idea behind mineral carbon dioxide sequestration is to replicate natural weathering processes, where silicate-based minerals, such as steelmaking slags, containing calcium or magnesium transform into calcium or magnesium carbonates [3,13,14]:



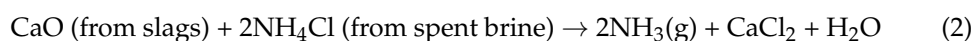
Mineral CO₂ sequestration, while effective, requires substantial amounts of calcium/magnesium minerals, although global sources exist [15,16]. An attractive solution lies in using industrial solid waste, such as slags and combustion residues, rich in calcium and readily available near CO₂ sources [3]. Unlike primary minerals, these waste materials are highly reactive, making them cost-efficient options that could reduce the energy consumption associated with mineral CO₂ sequestration [17,18].

This study focuses on a multifaceted approach to integrating slags from steelmaking with saline brines in CO₂ sequestration. Saline brines, which are abundant and often considered waste, can be utilized effectively in industrial processes, reducing environmental impacts, as they have an enormous capacity for industrial CO₂ storage [19–21]. CO₂-saturated brine descends to the lower depth of the aquifer because of the density variance after the CO₂ injection phase [22].

One propitious method for capturing CO₂ in saline brine is using chemical solvents, such as liquid ammonia [23]. While liquid NH₃ helps in CO₂ capture while utilizing saline water for the production of useful carbonates like baking soda (NaHCO₃) by the ammonia-based Solvay process, its presence poses health and environmental risks [24,25]. Therefore, efforts have been made to modify the Solvay process, aiming to replace ammonia and address these concerns [24,26–28]. Ali et al. [29] replaced liquid NH₃ in the Solvay process with different additives like Ca(OH)₂, KOH, and NH₄HCO₃ and compared their results using advanced techniques like XRD and SEM. The analysis revealed that using NH₄HCO₃ as an additive produced the highest-quality NaHCO₃, along with moderate amounts of Na₂CO₃.

The present work was conducted to combine the modified Solvay process and steelmaking waste elements to create a synergistic system. The novelty of the work is in exploring the multifaceted utility of steelmaking slags, aiming to leverage their properties in: (1) investigating the potential of slags to efficiently regenerate ammonium from the spent brine; (2) experimenting with slag as co-reagents in the bicarbonate production process, strategically designed to decrease the reliance on ammonium, thus optimizing the overall production efficiency; and (3) exploring the direct mineral carbonation of slags using residual brine from the bicarbonate synthesis.

In the context of sodium bicarbonate production and steelmaking, slags, rich in calcium oxide (CaO), are hypothesized in this study to potentially play a pivotal role in one or more of three key processes. Firstly, in the regeneration of ammonium from spent brine, ammonium chloride in the brine reacts with calcium oxide in the slags to elute as gaseous ammonia (NH₃) (Equation (2)) to be re-converted into NH₄HCO₃ via CO₂ capture. This regenerated ammonium could then be utilized in the bicarbonate synthesis reaction, minimizing the need for additional ammonium production.



Secondly, slags could act as a co-reagent by reacting with CO₂ and brine, forming sodium bicarbonate alongside ammonium (Equation (3)). This dual action can significantly reduce the requirement for ammonium, cutting both costs and environmental impacts associated with ammonia production, which often involves CO₂-emitting processes like natural gas burning. Additionally, these slags would facilitate mineral carbonation, a method of converting CO₂ into stable forms like calcium carbonate (CaCO₃).



Thirdly, by combining post-bicarbonate synthesis residual brine with slags, it would be expected that CO₂ would be extracted from the solution, reacting with the slags to form solid carbonates (Equation (1)). This process could effectively sequester CO₂ from steelmaking emissions, presenting a viable carbon capture and storage (CCS) strategy for hard-to-abate sectors such as ironmaking and steelmaking.

Integrating these components is aimed to optimize resource utilization, minimize waste, and significantly reduce the carbon footprint of industrial processes, aligning with the broader goals of sustainable development and environmental responsibility. The primary objective of the study was to evaluate the reactivity and the pH buffering capabilities of the steelmaking electric arc furnace (EAF) slag and compare it with two other abundant natural minerals, olivine, and kimberlite, to showcase its potential applications for the three aforementioned purposes, with particular emphasis on the ammonium regeneration step (Equation (2)). Geochemical modeling was further employed to predict the reactivity of the minerals in the study and to correlate to experimental findings for furthering mechanistic understanding.

2. Materials and Methods

2.1. Materials

The reactivity of three distinct minerals, EAF slag, olivine, and kimberlite, was examined in the presence of three aqueous solutions: ultrapure water (UPW; 18.2 MΩ·cm), brine containing ammonium bicarbonate (ABB), and brine containing potassium bicarbonate (PBB). The EAF slag utilized in this study was obtained from Natural Resources Canada (NRCan) and required crushing to achieve a particle size < 2 mm due to its coarse nature. Olivine, chosen for its relative purity and natural origin, was sourced from Nuova Cives (Italy) and used in its finely milled form. Kimberlite, a complex mine tailing known for its lower reactivity compared to olivine, was obtained from De Beers Canada from Northern Ontario and was sieved to <2 mm.

The chemical analyses of the materials examined in this study present distinct compositions for each specimen. The EAF slag is predominantly composed of oxides, including iron oxide (FeO), calcium oxide (CaO), silicon dioxide (SiO₂), aluminum oxide (Al₂O₃), and magnesium oxide (MgO) [30]. Variations in composition may occur based on the origin and processing methods. Considering the mineralogical aspects, EAF slag typically encompasses minerals like gehlenite (Ca₂Al₂SiO₇), larnite (Ca₂SiO₄), periclase (MgO), magnetite (Fe₃O₄), wüstite (FeO), hematite (Fe₂O₃), and other phases that can vary based on its specific composition and production process [31–33]. Olivine primarily comprises forsterite (Mg₂SiO₄) and fayalite (Fe₂SiO₄) as its major phase, potentially accompanied by minor constituents or impurities contingent upon its source [34]. Kimberlite, on the other hand, exhibits a varied mineralogical composition, comprising minerals such as spinel, phlogopite, diopside, among others, the specifics of which depend on geological context and the particular kimberlite deposit [35]. XRF (X-ray Fluorescence) analysis was specifically performed on the used EAF slag, olivine, and kimberlite to determine their elemental compositions, as shown in Table 1. It was conducted using Rigaku (Tokyo, Japan) Supermini 200 WDXRF, a sequential wavelength dispersive spectrometer and SuperQ software (version 6) by Malvern Panalytical (Worcestershire, United Kingdom) to facilitate accurate quantification.

Table 1. Chemical composition of EAF slag, olivine, and kimberlite determined by WDXRF and expressed as wt% oxides, and loss on ignition (LOI) determined by thermogravimetry.

(wt%)	Al ₂ O ₃	CaO	Fe ₂ O ₃	MgO	Na ₂ O	SO ₃	SiO ₂	LOI
EAF Slag	4.2	36.2	28.7	9.3	0.06	0.23	14.1	0.10
Olivine	2.1	2.1	9.2	38.7	0.21	0.07	39.1	7.3
Kimberlite	1.5	8.6	8.7	33.4	0.23	0.15	28.3	16.5

To further elucidate the physical attributes, the EAF slag, olivine, and kimberlite used during the study underwent a sieve analysis to determine particle size distribution. The findings revealed that the manually ground EAF slag possessed a coarser particle size compared to the other minerals, with olivine demonstrating the finest particle size. These findings are presented in Figure 1, depicting the differences in particle size distributions among the minerals. The ball-milled EAF slag was entirely passing 63 μm .

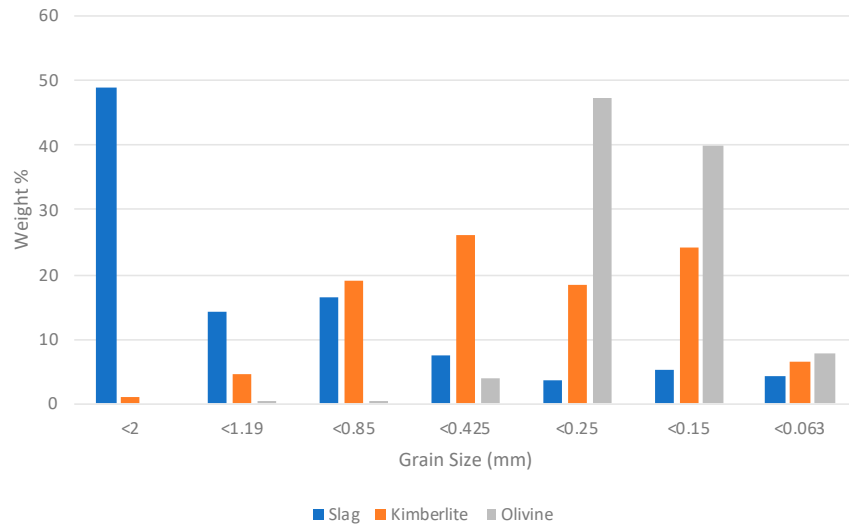


Figure 1. Particle size distribution of EAF slag, kimberlite, and olivine. Sizes indicate the passing size of each retained fraction and histogram values add to 100 wt%.

SEM (Scanning Electron Microscopy) analysis using the FEI (Hillsboro, OR, USA) Inspect S50 was conducted on both manually ground and ball-milled EAF slag to gain detailed insights on the morphologies of both the samples. Ball milling resulted in breakage and exfoliation of larger particles, as shown in Figure 2, with the slag not showing clear crystal morphology, indicating a high degree of amorphicity (later verified in XRD). Also, the SEM analysis showed the distinct morphology of slag compared to both olivine and kimberlite, with the latter having particles containing more clearly visible crystals.

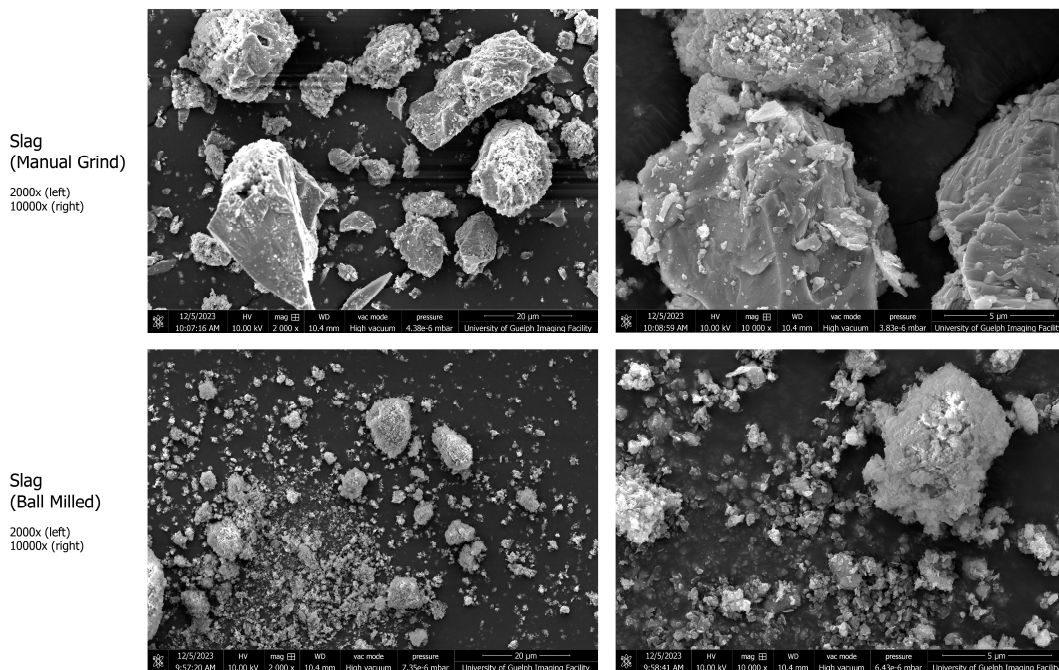


Figure 2. Cont.

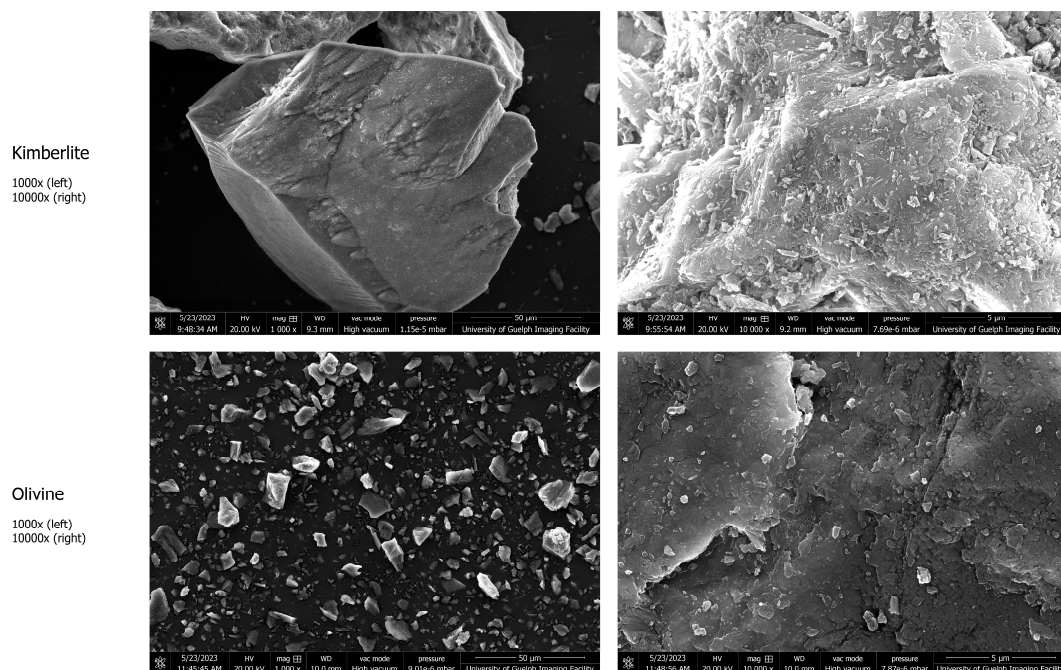


Figure 2. SEM images of manually ground EAF slag (**top row**), ball-milled EAF slag (**second row**), and as-received kimberlite (**third row**) and olivine (**bottom row**) before leaching. Left column shows lower magnification, and right column shows higher magnification.

The initial stage of the experiments involved preparing the brine solution. The chemicals used for brine preparation were sodium chloride NaCl (Fisher Scientific, with a purity level $\geq 90\%$), potassium hydroxide KOH (Fisher Scientific, with a purity level $\geq 85\%$ – 100%), sulfuric acid HCl (Fisher Scientific, with a purity level $\geq 36.5\%$ – 38%), and ammonium bicarbonate NH_4HCO_3 (Acros Organics, with a purity level $\geq 98\%$). These solutions were meticulously prepared to mirror the conditions explored in prior research (Ali et al. [29]), with brines containing an equivalent of 1.258 mol/L NaCl and the reagents NH_4HCO_3 and KHCO_3 at the same concentration [27]. The objective was to assess the minerals' reactivity concerning their influence on solution pH control and ion delivery, crucial factors in sodium bicarbonate NaHCO_3 synthesis. To simulate the varied pH levels these solutions might encounter during NaHCO_3 synthesis, the solutions were made more acidic by adding up to 1 mol/L HCl or made more basic by adding up to 1 mol/L NaOH. The pH stock solutions were prepared with ultrapure water, and the chemicals used were sulfuric acid HCl (Fisher Scientific, with a purity level $\geq 36.5\%$ – 38%) and sodium hydroxide NaOH (Fisher Scientific, with a purity level $\geq 50\%$).

2.2. Experimental Setup

The first experiment procedure involved mixing 5 g of each mineral with 100 mL of the corresponding solution. For each combination of mineral and solution (total of 9 combinations), 11 samples were prepared: one unaltered, devoid of any acidic or basic modifications, and 10 others subject to the influence of precisely controlled acid (0.001, 0.01, 0.05, 0.2, and 1 mol/L) and base (0.001, 0.01, 0.05, 0.2, and 1 mol/L) concentrations. This methodical approach yielded a total of 99 distinct compositions.

The resulting mixtures were shaken for 24 h in sealed bottles (Thermo Scientific Nalgene HDPE Centrifuge Bottles) using an orbital shaker. Following each experiment, the pH levels of the solutions were meticulously determined. The mixtures were then filtered through analytical filter paper, separating the solids from the liquid phase. The pH of each filtered liquid was measured to examine the change in pH levels. The collected solids underwent a thorough purification process, involving washing with ultrapure water to remove residual salts. Subsequently, the purified solids were dried at 105°C for 24 h in

the oven, ensuring the removal of any remaining moisture. The resulting dry mass was precisely measured, providing valuable insights into the reactivity and composition of the mineral-solution interactions. The residual solids underwent mineralogical analysis through X-ray diffraction (XRD) using the D8 Advance by Bruker (Massachusetts, United States) to identify their composition. The specific composition was quantified using the Rietveld refinement technique. Meanwhile, the liquid filtrate was acidified with 2% nitric acid and subjected to analysis via inductively coupled plasma optical emission spectroscopy (ICP-OES) using the Vista-PRO Simultaneous by Varian Inc. (Palo Alto, California, United States) to determine the concentrations of calcium, magnesium, and iron.

The second experiment was to observe the rate of regeneration of ammonium from spent brine. The experiment focused on creating an ammonium bicarbonate brine solution with a significantly reduced sodium concentration of 0.01258 mol/L, representing a 99% reduction compared to standard levels. In this procedure, 250 mL of the brine solution was heated on a hot plate to 50 °C and stirred at a constant rate of 400 rpm using a magnetic stirrer. Sequential additions of 2.5 g of the designated mineral were made at 5 min intervals, and pH measurements were taken before each addition. This process continued until a total of 50 g of the mineral had been added, maintaining a consistent liquid-to-solid (L/S) ratio of 5:1.

Another ammonium regeneration experiment was conducted to examine the necessary calcium leaching from slag to achieve optimal reactivity. Employing a setup similar to the second experiment but only with slag, the experiment maintained a similar sodium concentration, where a total of 250 mL of brine solution was heated to 50 °C. In this setup, the slag used was milled using a ball mill to achieve a particle size of <2 µm). In intervals of 30 min, 2.5 g portions of slag were systematically introduced until the total reached 50 g. Afterward, increments of 5 g of Ca(OH)₂ were added at 30 min intervals until a cumulative total of 10 g was reached, representing 20% of the weight concerning the initial slag used. Before each addition, the pH levels were recorded, providing data on the reaction dynamics. Following the addition of 50 g of slag and a subsequent 10 g of Ca(OH)₂, liquid samples were collected for dissolved NH₄⁺ testing to obtain ammonium concentration values for both samples.

2.3. Geochemical Modeling

The Geochemist's Workbench (GWB) software (Aqueous Solutions LLC, Champaign, IL, USA) was utilized for geochemical modeling purposes. Specifically, the Phase2 application within GWB was employed to generate phase diagrams for six minerals, namely, chrysotile (Mg₃Si₂O₅(OH)₄), fayalite (Fe₂SiO₄), forsterite (Mg₂SiO₄), gehlenite (Ca₂Al₂SiO₇), larnite (Ca₂SiO₄), and talc (Mg₃Si₄O₁₀(OH)₂). These minerals were chosen to represent the compositions found in EAF slag, olivine, and kimberlite. The modeling considered a solution composition equivalent to brine with ammonium bicarbonate, with variations in temperature from 0 to 100 °C and pH from the unadjusted value when the brine was mixed with 1 mol/L HCl, up to a pH of 14. As GWB performs equilibrium modeling, to ensure that the target mineral formed in at least a part of the phase diagram, competing silicate and carbonate minerals were suppressed.

3. Results and Discussion

Previous studies have indicated useful modified Solvay processes by using NaHCO₃, Ca(OH)₂, and KOH as buffering agents. In the present study, the most effective modified Solvay processes identified by Ali et al. [29] were combined with steelmaking slags to observe the reactivity of the mineral. The experiments would explore the reactivity of EAF slags in contrast to their industrial counterparts. Olivine and kimberlite were meticulously chosen to represent a broad spectrum of compositions found in industrial waste minerals. The use of XRD and ICP-OES techniques enhances the precision of process characterization, whereas geochemical modeling provides insights into the precipitate behavior of the minerals.

In the mineral reactivity experiments, the observed outcomes align closely with theoretical expectations. Figure 3 illustrates the change in pH and loss of mass at different acidic or basic concentrations for all three aqueous solutions. Minerals exhibited greater mass loss at lower pH levels and reduced mass loss at higher pH levels. Lower pH is known to facilitate the extraction of calcium, magnesium, and iron from silicate minerals, whereas higher pH enables the extraction of aluminum and silica, but to a lesser extent [36,37]. Notably, the ABB solution line appeared relatively linear for a wide range of acidity/basicity, potentially indicating a buffering effect enabled by the $\text{NH}_3/\text{NH}_4^+$ buffer pair. Such a buffering effect is made clearer when comparing the pH curves of ABB experiments to those of UPW, and such more stable and less basic pH conditions even under increased NaOH concentration can be potentially beneficial for ensuring mineral reactivity under a range of reaction conditions. Under UPW, the pH buffering effect of the slag is observed, with the pH remaining above 10 except for the two greatest acid additions, and the slag kept the pH of UPW up to 4 units higher than with the natural silicates, suggesting a substantial content of free alkaline earth metal oxides. Additionally, the PBB solution maintained a consistent pH of >10 for all minerals, except for the greatest acid addition, given that KOH is a stronger base than NH_4OH , suggesting limitations in mineral reactivity when reacted under PBB conditions. The observed mass changes confirm the expectation that more acidic conditions, namely, pH levels below 7.0, are needed to substantially cause the minerals to react. The mass change in slag was largely similar to that of natural minerals but slightly lower, suggesting its limited reactivity as compared to silicates. This difference can be attributed to the coarser particle size of the crushed slag (<2 mm), whereas the other minerals were already finely milled, with olivine being finer than kimberlite. However, as slag exhibited superior pH buffering capabilities compared to natural minerals, mineral reactivity appeared to be more influenced by pH effects than mere mass loss.

XRD analysis of slag, as depicted in Figure 4, highlights significant alterations in mineralogy during the reactivity experiments, showing observable changes under different conditions. The identified peaks in the XRD analysis were larnite (Ca_2SiO_4), hematite (Fe_2O_3), wüstite (FeO), magnetite (Fe_3O_4), gehlenite ($\text{Ca}_2\text{Al}(\text{AlSiO}_7)$), quartz (SiO_2), periclase (MgO), and calcite (CaCO_3). Firstly, the ball-milled slag diffraction signal, as a whole, shows higher intensity than the manually crushed slag, which can be a sign of amorphicity increase. Likewise, the base leaching appears to result in amorphous structures, which can occur as Si and Al are leached/alterred at high pH, leading to crystallinity changes/losses. Comparative observations between the blue lines (acidic condition) and red lines (neutral condition) depict distinct patterns, with the acidic condition displaying fewer peaks compared to the neutral one. In particular, it is noticed that calcite peaks reduced/disappeared from acidic samples, as would be expected by carbonate dissolution, whereas calcite peaks strengthened under basic conditions, especially when bicarbonates were used, showing that the slag carbonated during the leaching reactions. Moreover, intensification of certain peaks in the blue spectra suggests a significant impact on leaching under higher acid concentrations, leaving residual phases more concentrated than in the original slag. A closer examination reveals intensified and enlarged peaks indicative of residual solid iron oxides such as hematite, magnetite, and wüstite. This is further correlated by the increased overall intensity of blue spectra under UPW and PBB conditions, which is a fluorescence effect caused by increased iron content of the mineral [38]. Under ABB conditions, the fluorescence effect is less evident, which is likely a result of reduced leaching, given the aforementioned buffering effect of ammonium bicarbonate. Quantitative assessment via Rietveld refinement was found to be unreliable due to the complexity of these mineral samples, and particle size discrepancies may lead to preferential orientation and packing issues, impacting peak ratios and intensities.

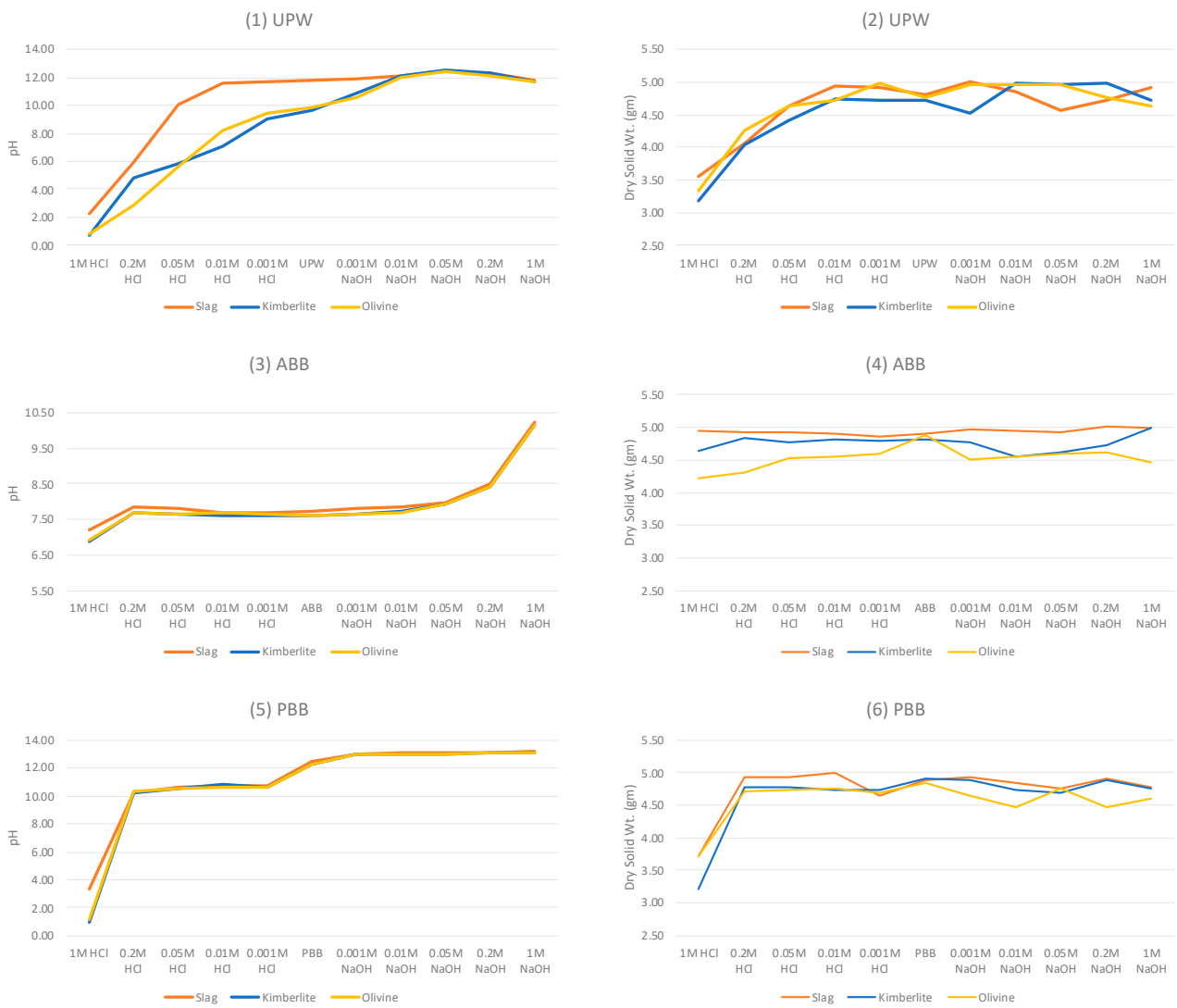


Figure 3. Change in pH (1,3,5) and change in mass of minerals after filtration (2,4,6) in different concentrations of acid (0.001, 0.01, 0.05, 0.2, and 1 mol/L), unaltered aqueous solution (UPW/ABB/PBB) and base (0.001, 0.01, 0.05, 0.2, and 1 mol/L) for EAF slag, olivine, and kimberlite in UPW (1,2), ABB (3,4), and PBB (5,6).

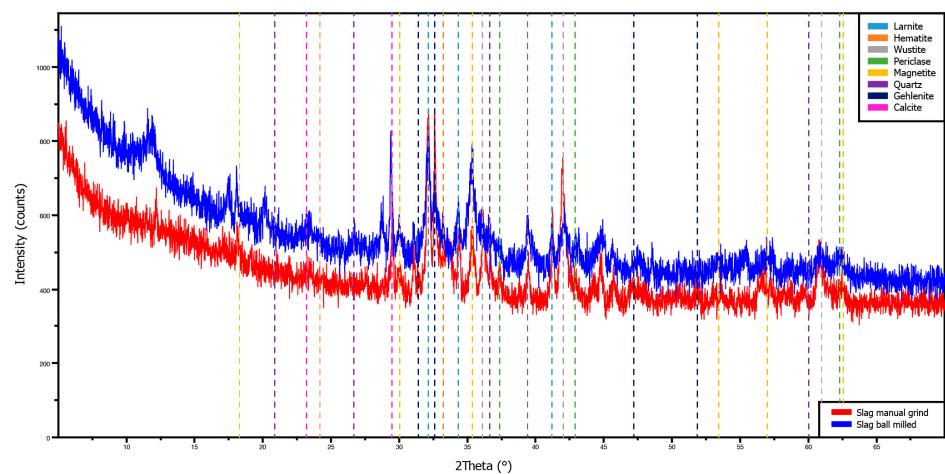


Figure 4. Cont.

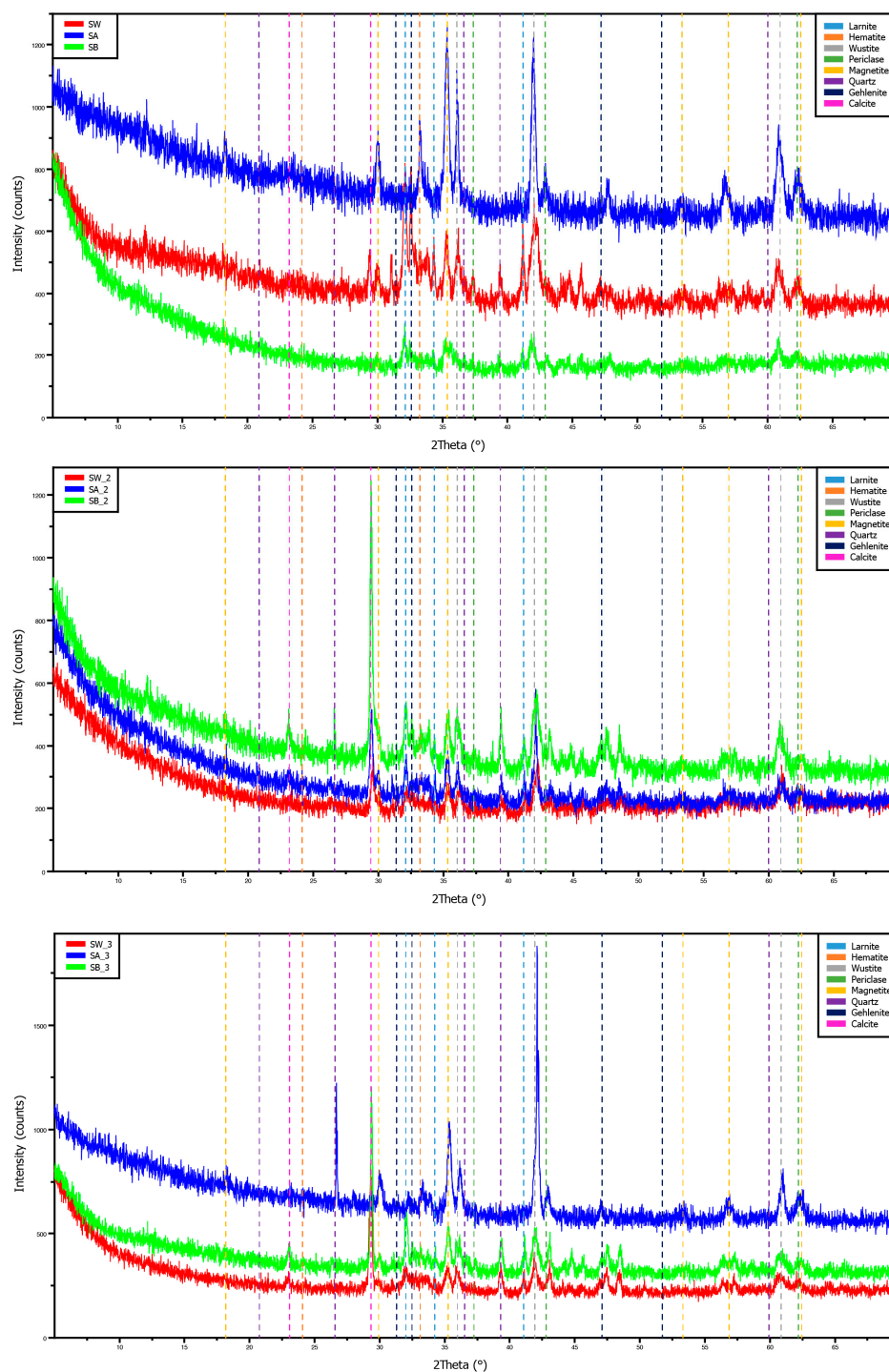


Figure 4. Stacked diffractograms from XRD analysis of the EAF slag (before (**first** subfigure) and after leaching) reacted in UPW (SW) (**second** subfigure), UPW with 1 mol/L HCl (SA), and UPW with 1 mol/L NaOH (SB). Samples with suffix_2 reacted in ABB (**third** subfigure) and with suffix_3 in PBB (**fourth** subfigure).

The ICP-OES data presented in Table 2 show the pivotal role of pH in the extraction of Ca, Fe, and Mg from the minerals. Due to its Ca-rich composition (Table 1) [39,40], slag exhibited the highest concentrations of Ca. Despite superior pH control, more Ca was extracted from slag than from natural minerals, validating the superior reactivity of the slag. Also, when the slag reacted with the acid, it resulted in extracted Ca and simultaneously helped to maintain the solution's pH level, highlighting the buffering

capacity of the slag. Consequently, the ICP-OES findings align with the pH results and are reinforced by the XRD discussions. In ABB, not much is leaching other than the Mg, seemingly suggesting an ion-exchange effect between NH_4^+ and Mg^{2+} , possibly from periclase/brucite. Ca, Fe, and Mg is leached in UPW and PBB when the concentration of HCl is relatively high. The mobilization of Fe from slag was notable, whereas Mg extraction was comparatively lower. Kimberlite, richer in Mg than Ca, displayed relatively high Ca mobilization, indicating substantial Ca speciation as carbonates rather than silicates. As anticipated, Mg mobilization from Mg-rich olivine [41] was the highest, followed by Fe, given olivine’s solid solution of forsterite and fayalite, and then Ca due to olivine’s low content [42] of Ca-silicates or -carbonates. Interestingly, olivine did not outperform kimberlite significantly, and this can be due to kimberlite’s varied mineral composition [43], which contains some highly reactive minerals such as spinel, phlogopite, diopside, among others commonly found in kimberlite deposits, and this occurred despite kimberlite’s coarser texture (Figure 1). Spinel, for instance, are known for their ability to exhibit high reactivity under certain conditions, contributing to the overall reactivity of kimberlite despite its coarser texture [44].

Table 2. The composition of the solutions used in the mineral reactivity experiments and the elemental concentrations of Ca, Fe, and Mg in the filtrate of the filtered solids, as determined by ICP-OES (samples with low concentration below the detection limit are shown as DT).

	Conc (M)	Ca	Fe	Mg	Ca	Fe	Mg	Ca	Fe	Mg	
		UPW			ABB			PBB			
Slag	1.000	16,081.20	5546.17	2097.62	262.53	DT	287.28	5415.03	1002.84	483.66	
	0.200	3199.02	180.48	198.12	38.19	37.52	370.29	DT	2.47	DT	
	0.050	789.45	DT	8.18	41.03	59.18	422.27	2.14	0.43	5.67	
	0.010	241.52	DT	DT	66.45	73.86	385.30	14.36	459.43	22.60	
	0.001	99.11	DT	DT	57.68	67.09	341.63	9.15	0.71	6.12	
	Brine	0.000	138.90	0.40	0.90	45.20	38.40	189.70	0.60	1.40	1.00
		0.001	82.35	0.09	0.04	36.66	40.34	228.28	3.09	0.89	1.05
		0.010	73.42	DT	DT	24.13	34.63	169.24	1.90	0.00	0.26
	NaOH	0.050	39.28	DT	DT	15.73	33.75	183.41	2.88	0.35	DT
		0.200	8.29	0.01	DT	7.89	27.74	76.79	3.23	0.35	DT
Kimberlite	1.000	23.88	DT	DT	2.05	1.15	72.33	8.77	0.91	DT	
	1.000	4862.14	963.88	4713.14	22.20	DT	245.99	2783.84	248.36	1769.26	
	0.200	3118.89	4.86	977.25	4.30	1.07	227.30	7.07	7.74	58.11	
	0.050	732.13	DT	164.36	5.94	DT	8.18	5.79	0.30	8.37	
	0.010	166.71	DT	34.93	0.05	2.29	168.68	0.81	DT	3.99	
	0.001	21.77	DT	3.86	1.10	5.09	136.78	1.88	DT	5.76	
	Brine	0.000	12.20	0.20	3.60	6.50	1.20	127.00	0.70	0.10	0.50
		0.001	41.03	0.18	7.01	5.98	1.37	120.70	3.06	DT	DT
		0.010	4.60	DT	0.59	6.50	2.34	121.58	2.32	DT	DT
	NaOH	0.050	5.20	DT	0.05	6.24	2.63	115.23	2.12	DT	DT
	0.200	1.64	DT	DT	4.47	2.26	105.04	2.46	DT	DT	
	1.000	37.36	DT	DT	4.05	1.24	88.88	5.60	0.08	DT	
Olivine	1.000	295.62	2791.75	7377.88	13.51	DT	254.28	151.75	832.65	3163.50	
	0.200	159.37	390.42	1872.18	0.50	0.99	238.24	7.88	18.70	199.77	
	0.050	662.64	181.81	540.39	0.69	1.63	236.15	1.55	0.17	38.73	
	0.010	47.32	DT	95.48	DT	1.26	226.25	DT	DT	DT	
	0.001	DT	DT	14.99	DT	1.46	229.66	2.37	0.05	DT	
	Brine	0.000	3.80	0.1	10.10	5.20	1.40	209.00	0.90	DT	1.60
		0.001	8.28	DT	1.43	5.52	1.33	205.78	3.06	DT	0.00
		0.010	14.75	1.70	22.08	5.57	1.34	201.89	2.69	DT	DT
	NaOH	0.050	3.67	DT	0.38	4.57	1.86	187.82	2.30	DT	DT
		0.200	0.13	DT	DT	4.13	2.25	103.21	2.72	DT	DT
	1.000	4.30	DT	DT	4.10	1.49	109.56	6.11	0.10	DT	

Green cells: largest concentrations (by greatest order of magnitude); Yellow cells: lower concentration as compared to green (second-greatest order of magnitude).

In the ammonium regeneration experiments, the results confirmed the earlier findings. From Figure 5, it can be observed that the slag, which is the most reactive mineral, effectively raised the solution’s pH quickly and significantly. Olivine performed next in terms of pH increase, whereas kimberlite, despite having reactive components, could not buffer the pH as effectively as olivine. The final pH of the olivine solution was only slightly lower than that of the slag, indicating olivine’s potential as a buffering agent, although slag remained superior.

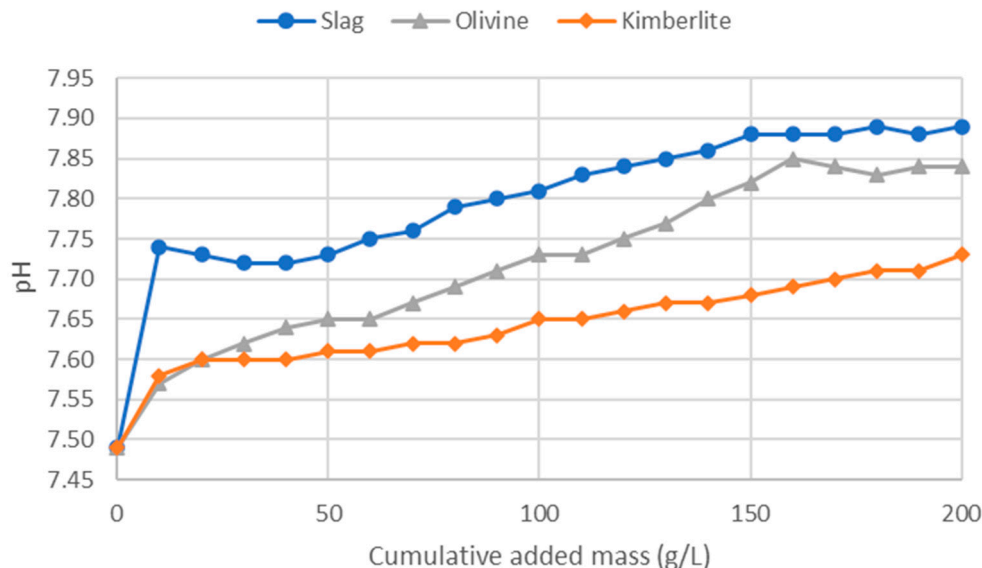


Figure 5. Ammonium regeneration experiment using slag, olivine, and kimberlite.

With a hypothesis that finer slag particles might perform better, potentially raising the pH above 8, the level needed to convert ammonium into ammonia according to Huang et al. [45], the next ammonium regeneration experiment was conducted. Therein, a finer ball-milled slag (Figure 2) was used, and it raised the pH above 8 after a cumulative added mass of 100 g/L, as illustrated in Figure 6.

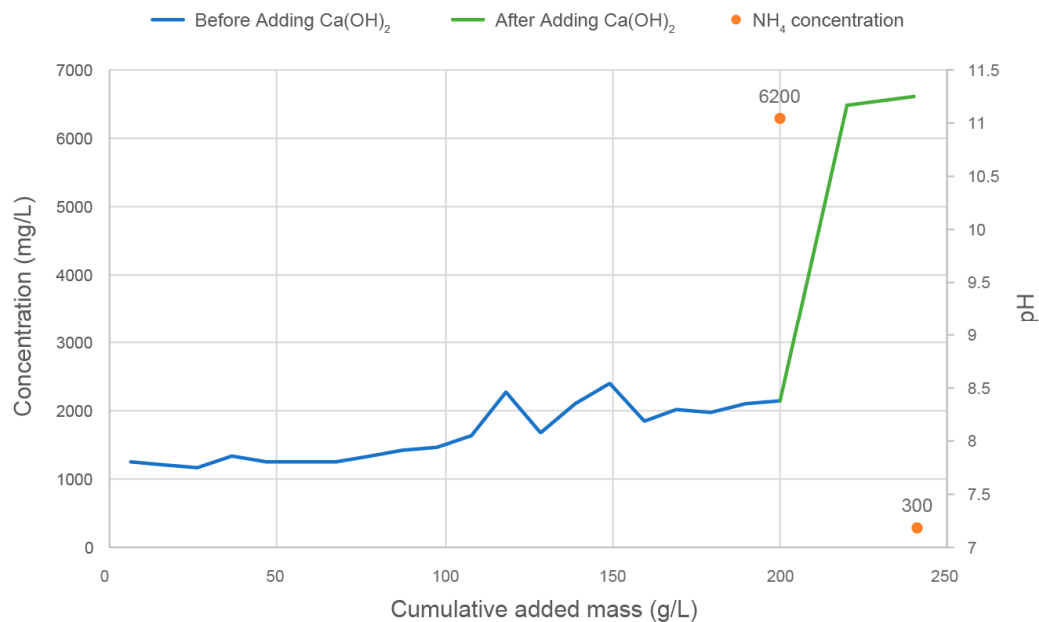


Figure 6. Ammonium regeneration experiment using finer ball-milled slag before and after adding Ca(OH)₂; concentration of NH₄⁺ in solution (initial value of 22,644 mg/L) and pH as a function of added mass of slag (up to 225 g/L) and Ca(OH)₂ (additional 25 g/L).

After adding $\text{Ca}(\text{OH})_2$ to examine the necessary calcium leaching from slag to achieve optimal reactivity, the pH rise to 11 indicates that the addition of $\text{Ca}(\text{OH})_2$ successfully promoted the desired chemical reactions (Equation (2)), emphasizing the significance of calcium leaching in enhancing the reactivity of the slag. The NH_4^+ concentration determination conducted to evaluate ammonium regeneration showcased distinct concentrations in the samples. The NH_4^+ concentration dropped from an initial value of 22,644 mg/L (1.258 M) to 6200 mg/L after slag addition, or 72.6% regeneration. Furthermore, with additional $\text{Ca}(\text{OH})_2$ addition, the NH_4^+ concentration dropped to 300 mg/L, or 98.7% NH_3 volatilization.

Geochemical modeling models based on equilibrium calculations rather than kinetics tend to overestimate reactivity, but they still yield comparable results (listed in Figure 7). Notably, larnite and gehlenite, minerals commonly found in slags [32], exhibit the least stability, explaining their reactivity below a pH of approximately 11. Forsterite, reactive below a pH of about 9, follows in terms of reactivity, whereas fayalite, also present in olivine, demonstrates lesser reactivity [46]. However, due to the solid solutions formed by these minerals, the reaction of solid solutions releases both Mg and Fe congruently, aligning with the ICP-OES results. Hydrated magnesium silicate minerals like chrysotile and talc exhibit lower reactivity compared to calcium silicate minerals, reacting only at a pH below approximately 8 or even 7, as per the equilibrium modeling results and kinetic modeling studies [14]. When these minerals coexist within olivine, they are known to impede its reactivity, showing that reactivity hindrances at the particle scale require specific intensification approaches that cannot be overcome at the process scale, when considering the multi-scale nature of mineral carbonation reactions [47]. Kimberlite, rich in these minerals, exhibits adequate reactivity in the experiments, due to the presence of minor reactive phases like carbonates.

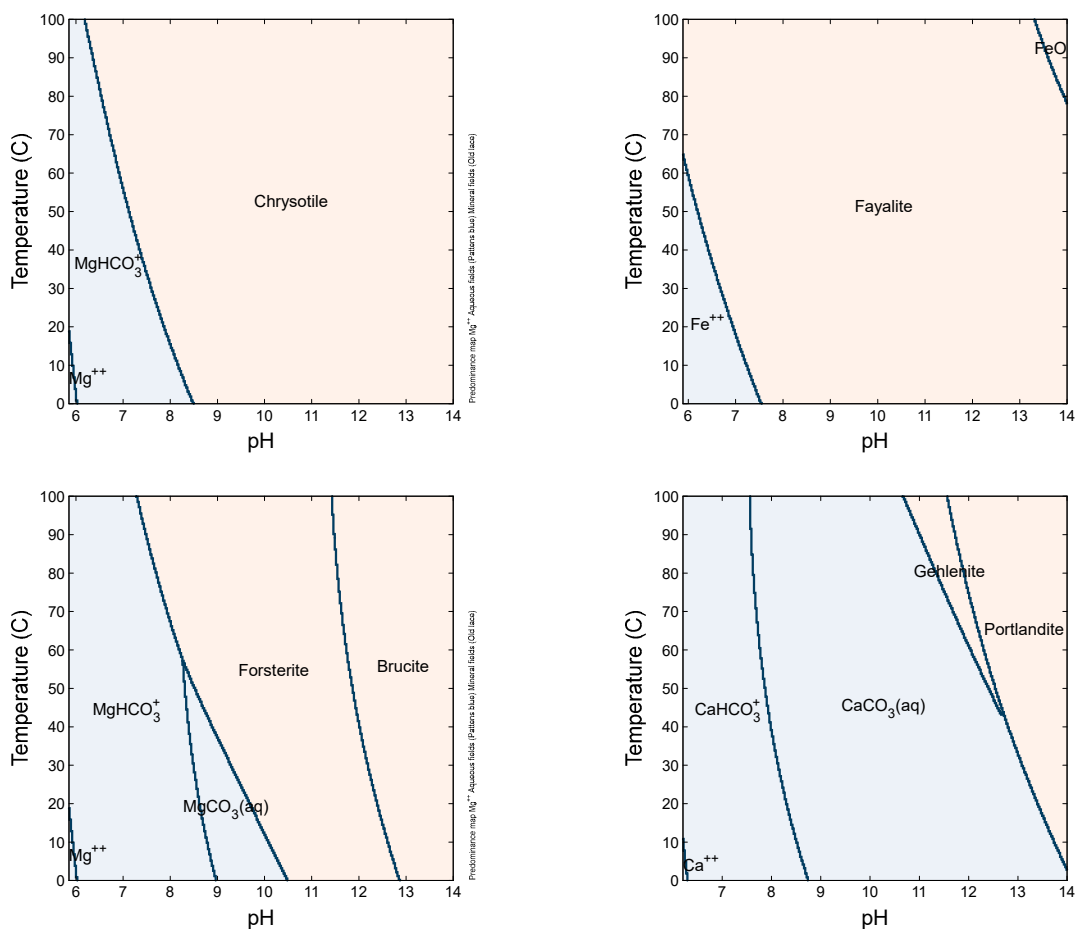


Figure 7. Cont.

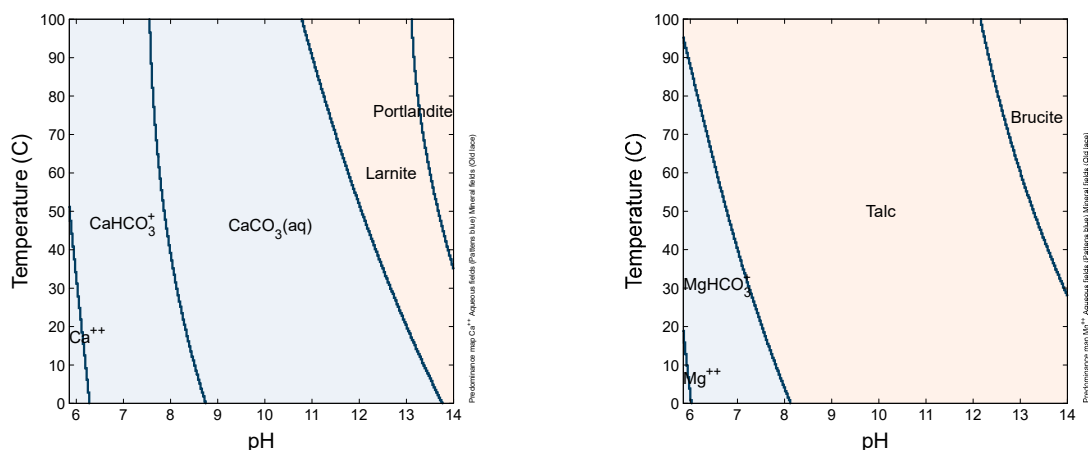


Figure 7. Phase diagrams of chrysotile (as Mg), fayalite (as Fe), forsterite (as Mg), gehlenite (as Ca), larnite (as Ca), and talc (as Mg) obtained from Geochemist's Workbench. Tan-colored regions indicate the dominant speciation of the element is a mineral, and blue-colored regions indicate the soluble species is dominant. Lines indicate transition regions.

4. Conclusions

In conclusion, this study presents a pioneering approach that integrates the modified Solvay process for sodium bicarbonate synthesis with steelmaking slags, addressing both CO₂ sequestration and reagent regeneration in a synergistic system. The pressing need to mitigate industrial CO₂ emissions, especially from the steel sector, finds a potential solution in mineral carbonation. Utilizing industrial solid waste, such as slags, in mineral carbonation processes can significantly reduce the carbon footprint associated with CO₂ capture and storage.

The reactivity experiments revealed intricate insights into the behavior of EAF slag, olivine, and kimberlite in varied pH conditions. The results demonstrated that mineral reactivity is intricately linked to pH effects, with pH playing a pivotal role in the extraction of key elements like calcium, magnesium, and iron from these minerals. The superior buffering capacity of EAF slag, especially in ammonium regeneration experiments, showcases its potential as a versatile and efficient material for CO₂ sequestration processes. Additionally, the finer particle size of the slag exhibited enhanced reactivity, indicating the importance of particle size in reactivity enhancement. Incorporating advanced analytical techniques such as XRD and ICP-OES further enhanced the precision of our study, enabling a comprehensive understanding of mineralogical alterations and elemental concentrations. Geochemical modeling also provided valuable insights into the behavior of minerals under varied pH conditions, aligning well with the experimental results. Notably, the presence of minerals like larnite and gehlenite in slags contributes significantly to their reactivity, suggesting potential avenues for optimizing industrial waste materials for CO₂ sequestration. These findings highlight the importance of understanding mineralogical compositions and their influences on reactivity, paving the way for tailored approaches in industrial CO₂ capture and storage strategies. In summary, the project findings suggest that using slag as a buffering agent in ammonium regeneration is a more effective application than its use in the sodium bicarbonate synthesis process. Additionally, as the slag only partially reacts, the remaining solid could be utilized to accelerate mineral carbonation processes, aiding in the sequestration of more CO₂. To advance this research, future studies should delve into these processes in detail and assess the overall energy requirements and carbon footprint associated with them.

Lastly, by minimizing waste, optimizing reagent usage, and enhancing CO₂ sequestration efficiency, this integrated approach not only contributes to mitigating climate change but also aligns with the principles of circular economy and sustainable industrial practices. In essence, these findings represent a significant step towards more sustainable, efficient, and economically viable solutions for reducing industrial carbon emissions, ultimately contributing to global efforts in combatting climate change.

Author Contributions: Conceptualization, R.M.S.; methodology, S.M.A., A.A. and R.M.S.; investigation, S.M.A. and A.A.; writing—original draft preparation, S.M.A.; writing—review and editing, R.M.S.; supervision, R.M.S.; project administration, R.M.S.; funding acquisition, R.M.S. All authors have read and agreed to the published version of the manuscript.

Funding: This work is supported by the Program of Energy Research and Development of Canada. The authors acknowledge funding received from the Natural Science and Engineering Research Council (Discovery Grant).

Data Availability Statement: The data presented in this study are available on request from the corresponding author.

Acknowledgments: The authors are grateful for the laboratory assistance provided by doctoral students Reza Khalidy and Hiral Jariwala and for the slag sourcing and funding securement facilitated by Jinsheng Wang of CanmetENERGY (Natural Resources Canada).

Conflicts of Interest: The authors declare no conflicts of interest.

References

1. Letcher, T.M. 1—Global warming—A complex situation. In *Climate Change*, 3rd ed.; Elsevier: Amsterdam, The Netherlands, 2021; pp. 3–17. [CrossRef]
2. Miao, E.; Du, Y.; Wang, H.; Xiong, Z.; Zhao, Y.; Zhang, J. Experimental study and kinetics on CO₂ mineral sequestration by the direct aqueous carbonation of pepper stalk ash. *Fuel* **2021**, *303*, 121230. [CrossRef]
3. Huijgen, W.J.; Witkamp, G.J.; Comans, R.N. Mineral CO₂ Sequestration by Steel Slag Carbonation. *Environ. Sci. Technol.* **2005**, *39*, 9676–9682. [CrossRef]
4. US Department of Commerce. Global Monitoring Laboratory—Carbon Cycle Greenhouse Gases. GML. 1 October 2005. Available online: <https://gml.noaa.gov/ccgg/trends/> (accessed on 11 November 2023).
5. Rammer, B.; Millner, R.; Boehm, C. Comparing the CO₂ Emissions of Different Steelmaking Routes. *BHM Berg-und Hüttenmännische Monatshefte*. **2017**, *162*, 7–13. [CrossRef]
6. World Steel Association. World Steel in Figures 2021. Available online: <https://worldsteel.org/steel-topics/statistics/World-Steel-in-Figures/> (accessed on 10 October 2023).
7. Mapelli, C.; Dall'Osto, G.; Mombelli, D.; Barella, S.; Gruttadauria, A. Future Scenarios for Reducing Emissions and Consumption in the Italian Steelmaking Industry. *Steel Res. Int.* **2022**, *93*, 2100631. [CrossRef]
8. International Energy Agency. Greenhouse Gas Emissions from Major Industrial Sources III-Iron and Steel Production Report PH3/30. Available online: https://ieaghg.org/docs/General_Docs/Reports/PH3-30%20iron-steel.pdf (accessed on 10 October 2023).
9. International Energy Agency. Iron and Steel Technology Roadmap towards More Sustainable Steelmaking Part of the Energy Technology Perspectives Series. Available online: <https://www.iea.org/reports/iron-and-steel-technology-roadmap> (accessed on 23 October 2023).
10. Lackner, K.S. A Guide to CO₂ Sequestration. *Science* **2023**, *300*, 1677–1678. [CrossRef]
11. Chai, Y.; Chalouati, S.; Fantucci, H.; Santos, R. Accelerated weathering and carbonation (mild to intensified) of natural Canadian silicates (kimberlite and wollastonite) for CO₂ sequestration. *Crystals* **2021**, *11*, 1584. [CrossRef]
12. Zhang, Y.; Yu, L.; Cui, K.; Wang, H.; Fu, T. Carbon capture and storage technology by steel-making slags: Recent progress and future challenges. *Chem. Eng. J.* **2023**, *455*, 140552. [CrossRef]
13. Eloneva, S.; Teir, S.; Revitzer, H.; Salminen, J.; Said, A.; Fogelholm, C.-J.; Zevenhoven, R. Reduction of CO₂ Emissions from Steel Plants by Using Steelmaking Slags for Production of Marketable Calcium Carbonate. *Steel Res. Int.* **2010**, *80*, 415–421. [CrossRef]
14. Haque, F.; Khalidy, R.; Chiang, Y.; Santos, R. Constraining the capacity of global croplands to CO₂ drawdown via mineral weathering. *ACS Earth Space Chem.* **2023**, *7*, 1294–1305. [CrossRef]
15. Gadikota, G.; Matter, J.; Kelemen, P.; Brady, P.; Park, A.-H. Elucidating the differences in the carbon mineralization behaviors of calcium and magnesium bearing aluminosilicates and magnesium silicates for CO₂ storage. *Fuel* **2020**, *277*, 117900. [CrossRef]
16. Woodall, C.; Lu, X.; Dipple, G.; Wilcox, J. Carbon Mineralization with North American PGM Mine Tailings—Characterization and Reactivity Analysis. *Minerals* **2021**, *11*, 844. [CrossRef]
17. Meima, J.A.; van der Weijden, R.; Eighmy, T.T.; Comans, R.N.J. Carbonation processes in municipal solid waste incinerator bottom ash and their effect on the leaching of copper and molybdenum. *Appl. Geochem.* **2002**, *17*, 1503–1513. [CrossRef]
18. Chalouati, S.; Yoosefdoost, A.; Chiang, Y.; Santos, R. Intensified mineral carbonation of natural Canadian silicates using simultaneous ball milling. *Int. J. Coal Geol.* **2023**, *277*, 104332. [CrossRef]
19. Al Hameli, F.; Belhaj, H.; Al Dhuhoori, M. CO₂ Sequestration Overview in Geological Formations: Trapping Mechanisms Matrix Assessment. *Energies* **2022**, *15*, 7805. [CrossRef]
20. Sun, Y.; Payton, R.L.; Hier-Majumder, S.; Kingdon, A. Geological Carbon Sequestration by Reactive Infiltration Instability. *Front. Earth Sci.* **2020**, *8*, 533588. [CrossRef]

21. Zhang, N.; Chai, Y.; Santos, R.; Šiller, L. Advances in process development of aqueous CO₂ mineralisation towards scalability. *J. Environ. Chem. Eng.* **2020**, *8*, 104453. [CrossRef]
22. Alexander, D.; Boodlal, D. Evaluating the effects of CO₂ Injection in Faulted Saline Aquifers. *Energy Procedia* **2014**, *63*, 3012–3021. [CrossRef]
23. Bai, H.; Yeh, A.C. Removal of CO₂ Greenhouse Gas by Ammonia Scrubbing. *Ind. Eng. Chem. Res.* **1997**, *30*, 2490–2493. [CrossRef]
24. Cormos, A.-M.; Dinca, C.; Petrescu, L.; Chisalita, D.A.; Szima, S.; Cormos, C.-C. Carbon capture and utilisation technologies applied to energy conversion systems and other energy-intensive industrial applications. *Fuel* **2018**, *211*, 883–890. [CrossRef]
25. Carson, P.; Mumford, C. Hazardous Chemicals Handbook, Library of Congress Cataloguing in Publication Data. 2002. Available online: <http://ccc.chem.pitt.edu/wipf/Web/HCH> (accessed on 10 October 2023).
26. Setayeshmanesh, T.; Parivazh, M.M.; Abbasi, M.; Osfouri, S.; Dianat, M.J.; Akrami, M. Reducing the Environmental Impacts of Desalination Reject Brine Using Modified Solvay Process Based on Calcium Oxide. *Sustainability* **2022**, *14*, 2298. [CrossRef]
27. Wang, Q.; Li, Z. A modified Solvay process with low-temperature calcination of NaHCO₃ using monoethanolamine: Solubility determination and thermodynamic modeling. *AIChE J.* **2019**, *65*, e16701. [CrossRef]
28. Mourad, A.A.-H.; Mohammad, A.F.; Al-Marzouqi, A.H.; El-Naas, M.H.; Al-Marzouqi, M.H.; Altarawneh, M. CO₂ capture and ions removal through reaction with potassium hydroxide in desalination reject brine: Statistical optimization. *Chem. Eng. Process. Process Intensif.* **2022**, *170*, 108722. [CrossRef]
29. Ali, A.; Mendes, C.E.; de Melo, L.G.; Wang, J.; Santos, R.M. Production of Sodium Bicarbonate with Saline Brine and CO₂ Co-Utilization: Comparing Modified Solvay Approaches. *Crystals* **2023**, *13*, 470. [CrossRef]
30. Mombelli, D.; Mapelli, C.; Barella, S.; Gruttadauria, A.; Di Landro, U. Analysis of Electric Arc Furnace Slag. *Steel Res. Int.* **2012**, *83*, 1012–1019. [CrossRef]
31. Adegoloye, G.; Beaucour, A.-L.; Ortola, S.; Noumowe, A. Mineralogical composition of EAF slag and stabilised AOD slag aggregates and dimensional stability of slag aggregate concretes. *Constr. Build. Mater.* **2016**, *115*, 171–178. [CrossRef]
32. Mombelli, D.; Mapelli, C.; Barella, S.; Di Cecca, C.; Le Saout, G.; Garcia-Diaz, E. The effect of microstructure on the leaching behaviour of electric arc furnace (EAF) carbon steel slag. *Process Saf. Environ. Prot.* **2016**, *102*, 810–821. [CrossRef]
33. Menad, N.E.; Kana, N.; Seron, A.; Kanari, N. New EAF Slag Characterization Methodology for Strategic Metal Recovery. *Materials* **2021**, *14*, 1513. [CrossRef]
34. Pamato, M.G.; Nestola, F.; Novella, D.; Smyth, J.R.; Pasqual, D.; Gatta, G.D.; Alvaro, M.; Secco, L. The High-Pressure Structural Evolution of Olivine along the Forsterite–Fayalite Join. *Minerals* **2019**, *9*, 790. [CrossRef]
35. Emeleus, C.H.; Andrews, J.R. Mineralogy and petrology of kimberlite dyke and sheet intrusions and included peridotite xenoliths from South-West Greenland. *Phys. Chem. Earth* **1975**, *9*, 179–197. [CrossRef]
36. Owais, M.; Järvinen, M.; Taskinen, P.; Said, A. Experimental study on the extraction of calcium, magnesium, vanadium and silicon from steelmaking slags for improved mineral carbonation of CO₂. *J. CO₂ Util.* **2019**, *31*, 1–7. [CrossRef]
37. Hermosilla, D.; Ordóñez, R.; Blanco, L.; de la Fuente, E.; Blanco, Á. pH and Particle Structure Effects on Silica Removal by Coagulation. *Chem. Eng. Technol.* **2012**, *35*, 1632–1640. [CrossRef]
38. Hansford, G.M.; Turner, S.M.R.; Staab, D.; Vernon, D. The suppression of fluorescence peaks in energy-dispersive X-ray diffraction. *J. Appl. Crystallogr.* **2014**, *47*, 1708–1715. [CrossRef]
39. Piatak, N.M.; Parsons, M.B.; Seal, R.R. Characteristics and environmental aspects of slag: A review. *Appl. Geochem.* **2015**, *57*, 236–266. [CrossRef]
40. Said, A.; Mattila, H.-P.; Järvinen, M.; Zevenhoven, R. Production of precipitated calcium carbonate (PCC) from steelmaking slag for fixation of CO₂. *Appl. Energy* **2013**, *112*, 765–771. [CrossRef]
41. Sunshine, J.M.; Pieters, C.M. Determining the composition of olivine from reflectance spectroscopy. *J. Geophys. Res. Planets* **1998**, *103*, 1367513688. [CrossRef]
42. Kamenetsky, V.S.; Elburg, M.; Arculus, R.; Thomas, R. Magmatic origin of low-Ca olivine in subduction-related magmas: Co-existence of contrasting magmas. *Chem. Geol.* **2006**, *233*, 346–357. [CrossRef]
43. Wilson, L.; Head, J.W., II. An integrated model of kimberlite ascent and eruption. *Nature* **2007**, *447*, 53–57. [CrossRef]
44. Grégoire, M.; Tinguely, C.; Bell, D.R.; Roex, A.L. Spinel lherzolite xenoliths from the Premier kimberlite (Kaapvaal craton, South Africa): Nature and evolution of the shallow upper mantle beneath the Bushveld complex. *Lithos* **2005**, *84*, 185–205. [CrossRef]
45. Huang, J.-C.; Shang, C. Air Stripping. Advanced Physicochemical Treatment Processes. In *Handbook of Environmental Engineering*; Wang, L.K., Hung, Y.T., Shamma, N.K., Eds.; Humana Press: Totowa, NJ, USA, 2006; Volume 4. [CrossRef]
46. Béarat, H.; McKelvy, M.J.; Chizmeshya, A.V.G.; Gormley, D.; Nunez, R.; Carpenter, R.W.; Squires, K.; Wolf, G.H. Carbon Sequestration via Aqueous Olivine Mineral Carbonation: Role of Passivating Layer Formation. *Environ. Sci. Technol.* **2006**, *40*, 4802–4808. [CrossRef]
47. Santos, R.; Zhang, N.; Bakhshoodeh, R. Multiscale process intensification of waste valorization reactions. *Acc. Chem. Res.* **2023**, *56*, 2606–2619. [CrossRef]

Disclaimer/Publisher’s Note: The statements, opinions and data contained in all publications are solely those of the individual author(s) and contributor(s) and not of MDPI and/or the editor(s). MDPI and/or the editor(s) disclaim responsibility for any injury to people or property resulting from any ideas, methods, instructions or products referred to in the content.